A study of the successive phase transitions in $KTa_{0.93}Nb_{0.07}O_3$ by light scattering, dielectric permittivity and light diffraction measurements

1994 J. Phys.: Condens. Matter 6 1965

(http://iopscience.iop.org/0953-8984/6/10/015)

J. Phys.: Condens. Matter 6 (1994) 1965–1984. Printed in the UK

A study of the successive phase transitions in $KTa_{0.93}Nb_{0.07}O_3$ by light scattering, dielectric permittivity and light diffraction measurements

Elghalia Bouziane†, Marc Fontana† and Wolfgang Kleemann‡

† Laboratoire Matériaux Optiques à Propriétés Spécifiques, CLOES, University of Metz and Supelec, 2 Rue Belin, 57078 Metz Cédex 3, France

‡ Laboratorium für Angewandte Physik, Universität Duisburg, Lotharstrasse 65, D-47057 Duisburg, Germany

Received 27 October 1993

Abstract. The phase transitions in $KTa_{1-x}Nb_xO_3$ (KTN) with $x = 0.076$ have been investigated by various methods. The modifications of the light diffraction patterns recorded as a function of the temperature reveal three successive changes in symmetry. These results are consistent with the anomalies detected for the same crystal in the temperature dependence of both the dielectric permittivity and the light transmission and confirm the sequence of cubic–tetragonal–orthorhombic–rhombohedral structural phase transitions. A careful analysis of the temperature dependence of the integrated intensity for each transverse optical phonon line below the cubic–tetragonal transition shows similar anomalies at each transition. These transitions are preceded in the cubic phase by the formation of precursor clusters as in very dilute KTN crystals. These microregions are evidenced from the occurrence of intense quasi-elastic scattering well above the first transition and thereby of the activated phonon density of states bands.

1. Introduction

Much current interest is devoted to the influence of defects in highly polarizable systems [1, 2]. In particular the mechanism of phase transitions that yield either a dipole glass state or a long-range ferroelectric ordering has been the object of numerous investigations and discussions.

The phase transitions caused by niobium ions in potassium tantalate have been widely investigated by various experimental techniques. In the solid solutions of $KTa_{1-x}Nb_xO_3$ (KTN) it is generally accepted that a ferroelectric phase transition takes place from the cubic to the rhombohedral phase above the critical concentration $x = 0.008$. The sequence of cubic–tetragonal–orthorhombic–rhombohedral (C–T–O–R) phase transitions is expected as in pure $KNbO_3$ for concentrations above a multicritical point, which was reported to correspond to $x = 0.05$ [3] and, more recently, to $0.02 < x < 0.03$ [4].

For crystals with low Nb content ($0.08 < x < 0.02$) some deviations in physical quantities such as the permittivity or the elastic compliance were attributed to quantum fluctuation effects [3, 5]. Whereas some results can clearly be interpreted within a displacive ferroelectric transition picture [6], other data reveal the role of Nb to be compatible with a situation close to that found in spin glasses [7, 8].

In fact, our recent Raman [9] and dielectric [10] measurements carried out at various Nb concentrations also seem to favour a description based upon the coexistence of glassy

0953-8984/94/101965+20$19.50

behaviour and long-range ferroelectric order at low concentrations [9–11]. It will be shown in this paper that this is also valid to some degree for higher concentrations.

In this paper we present results that are, for the first time, simultaneously obtained by dielectric, Raman scattering, light diffraction and transmission measurements on the same KTN crystal with a relative large concentration $x = 0.076$. Our aim is to study

(i) the evidence for the expected C–T–O–R phase transitions on a macroscopic scale,

(ii) the precursor phenomena in regard to the results carried out for low concentrations and

(iii) the relationship between the changes in the dynamics of the $KTaO_3$ lattice, the Nb cluster fluctuations and the structural transformations.

Raman studies in KTN with low Nb concentration $x = 0.02$ [12, 9] or $x = 0.012$ [8, 11] as well as in pure $KTaO_3$ [13] reveal the presence of unexpected lines above T_c, which are attributed to microscopic ferroelectric regions. The investigation of these precursor effects also merits particular attention for larger Nb concentrations in order to clarify their relation with the mechanism of successive phase transitions.

In our study we perform light scattering experiments in order to detect Raman lines above T_c, and to evidence polar clusters in the quasi-elastic frequency range.

We introduce an additional technique, which is able to directly monitor the temperatures at which a structural change occurs on a macroscopic scale. Light diffraction is a sensitive probe to determine structural phase transitions and the corresponding change of ferroelectric domains. This technique is complementary to the dielectric susceptibility measurements, which generally indicate the transition temperatures by the occurrence of maxima.

Earlier studies reported on KTN with large concentrations will be critically reviewed. Light scattering measurements for $x = 0.26$ and $x = 0.28$ [14] gave evidence of a central peak above T_{c1}, which was shown to be consistent with the eight-site order–disorder model invoked for $KNbO_3$ [15], whereas the appearance of the hard phonon around 200 cm^{-1} was attributed to a simple phase transition of the C–T type. Toulouse *et al* [16] carried out both dielectric and spontaneous polarization measurements for $x = 0.16$. Data show the appearance of a non-zero polarization 20 K above the temperature corresponding to the maximum of permittivity ϵ. Moreover, ϵ reveals only two anomalies instead of three and its main peak does not seem to correspond to a phase transition [16].

2. Experimental results

2.1. Light diffraction and transmission measurements

Owing to the orientational degeneracy of the ferroelectric order parameter, the phase transitions of KTN are accompanied by domain formation as observed in $KNbO_3$ and $BaTiO_3$ [17]. Owing to the changes of the refractive indices from one domain to the other the appearance of light diffraction is expected if the domain arrangement is quasi-regular with periods of the order of the light wavelength. Very generally [18], different phases are characterized by different domain patterns. The study of their diffraction patterns may then provide valuable information upon successive phase transitions. In the present case they helped to determine at lease the transition temperatures. Significant changes were observed at 82.5, 78.5 and 74.5 K. Measurements were made on cooling, starting with the cubic phase above 83 K. Figure 1(a) is obtained at 100 K, showing merely one central spot, due to an

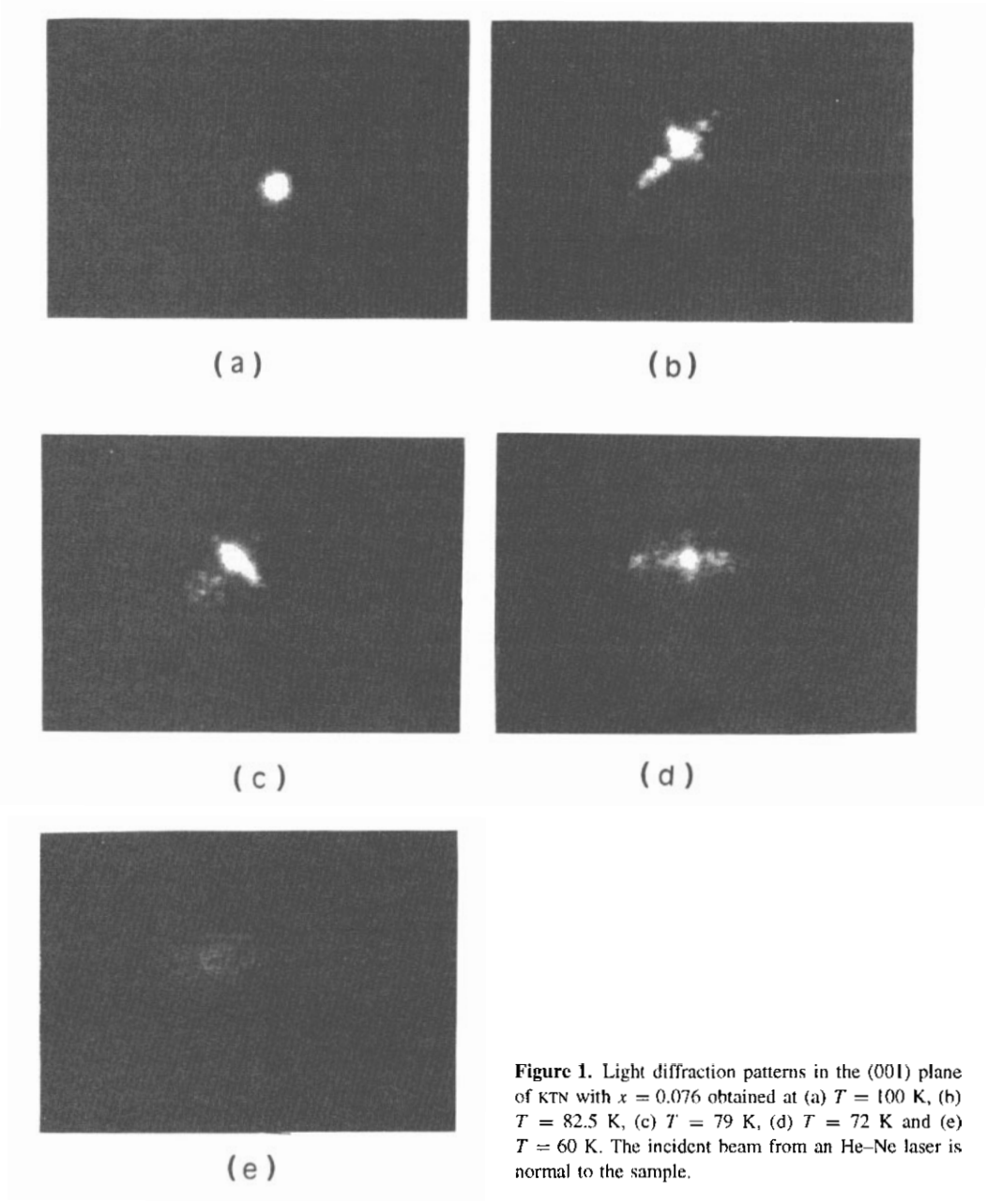

Figure 1. Light diffraction patterns in the (001) plane of KTN with $x = 0.076$ obtained at (a) $T = 100$ K, (b) $T = 82.5$ K, (c) $T = 79$ K, (d) $T = 72$ K and (e) $T = 60$ K. The incident beam from an He–Ne laser is normal to the sample.

He-Ne laser beam hitting the sample's (001) face along the [001] direction. Note that all orientations $\langle 1mn \rangle$ and planes $\{1mn\}$ will henceforth be related to the cubic parent phase.

Below 83 K, diffraction spots appear more or less symmetrically with respect to the central maximum aligned along the four $\langle 110 \rangle$ directions of the sample (figure 1(b)). Obviously quasi-periodic twin domains with alternating refractive indices and walls parallel to $\{\bar{1}10\}$ are forming. They are typical of the tetragonally distorted phase (as in $KNbO_3$ or $BaTiO_3$ [17]). The elongated polar c axis alternates between the [100] and [010] directions. The resulting phase grating has a square modulation of the birefringence varying between $n_c - n_a$ and $n_a - n_c$. It has been verified that diffraction is obtained under arbitrary

incident linear polarizations. Diffraction patterns similar to those shown in figure 1(b) were also observed for $KTaO_3$:Li ($x = 0.026$) in its tetragonal phase [18]. The stripe domain arrangement responsible for the diffraction pattern was directly observed by means of polarizing microscopy in the tetragonal phase of KTN ($x = 0.03$) within the range $42 < T < 44$ K [4]. Using thin phase grating arguments, the average domain widths are evaluated to be of the order of 10μm from figure 1(b).

The orthorhombic phase is indicated by typical new features. Below 79.5 K the $\langle 110 \rangle$ oriented diffraction cross becomes broadened by additional diffraction spots (figure 1(c)). Obviously the $\{\bar{1}10\}$ oriented domain walls form intersecting square lattices when projected onto the (001) plane. The broadened diffraction cross is characteristic of such two-dimensional phase gratings. Moreover, diffraction spots along $\langle 100 \rangle$ are expected. They are due to twin-domain gratings due to domains with the polar c axis along [110] and $[\bar{1}10]$ within the (001) plane. Surprisingly, the entire diffraction pattern of figure 1(c) shrinks on further cooling and coincides essentially with the central spot within $78 > T > 75$ K. Obviously considerable domain growth takes place within the narrow range of stability of the orthorhombic phase.

Dramatic changes of the diffraction pattern are observed at the transition into the rhombohedral phase. In the vicinity of 75 K, a new pattern with wings elongated along [100] and [010] appears (figure 1(d)). This corresponds to quasi-periodic twin-domain arrangements formed by the eight dipolar $\langle 111 \rangle$ species. One easily finds that the (100) and (010) planes correspond to neutral planes between these twins and thus form the domain walls. Again, the broadened cross hints at an intersecting twin-domain system. Interestingly, upon further cooling the diffraction cross loses its structure (indicating distinct grating constants). It transforms into a washed-out halo, which, however, still maintains the fourfold symmetry (figure 1(e)). Obviously, the rhombohedral domains tend to form fine-grained irregular arrangements, which may be considered as three-dimensional phase gratings. Very probably these gratings exhibit very effective Bragg diffraction [19], which attenuates the light beam to a large extent (see below).

Here we conclude that the different changes of the diffraction patterns are clear signatures of the successive phase transitions on decreasing temperature. The C–T, T–O and O–R transitions are found to occur at $T = 82.5$, 79 and 74.5 K, respectively.

This conclusion is corroborated by experiments under the application of electric field E the amplitude of which is 4 kV cm^{-1}, along the [010] direction. The external field induces domain alignment along its direction. It helps privileged domains to grow up to macroscopic size and to suppress the diffraction patterns. Only a central spot is observed for all temperatures from 100 K down to 73 K. The same pattern as obtained without field in figure 1(a) is detected. Below 73 K, however, in the rhombohedral phase, a diffuse scattering halo reappears (figure 2(a)). As is evident from figure 2(b), four of eight possible domains survive in the field and still give rise to diffraction.

We also studied the temperature dependence of the transmitted light intensity. We compare the transmitted light that has the polarization parallel ($I_\parallel$) or normal ($I_\perp$) to the polarization of the incident beam. Figure 3 shows the temperature dependence of both intensities, $I_\parallel$ and $I_\perp$.

The decrease of both $I_\parallel$ and $I_\perp$ within the temperature range from 100 K down to 85 K (close to $T_{c1} = 82.5$ K) is very probably due to the quasi-elastic light scattering revealing the existence of ferroelectric precursor clusters in the cubic phase. The same phenomenon is found in the Raman scattering experiment and will be discussed below (section 2.3). At the C–T as well as the T–O phase transition, $I_\parallel$ drops by steps from the initial intensity. Contrastingly, $I_\perp$ steeply increases at the C–T and T–O transitions. Clearly,

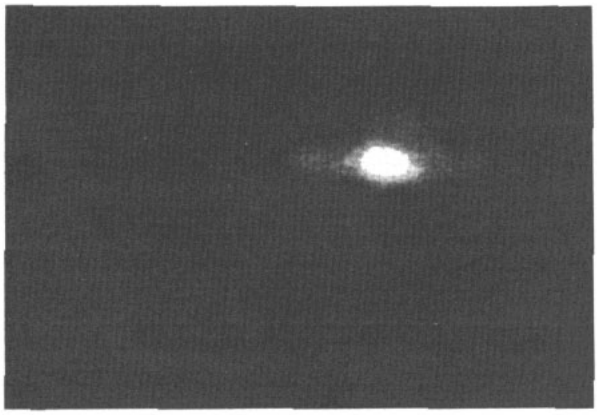

(a)

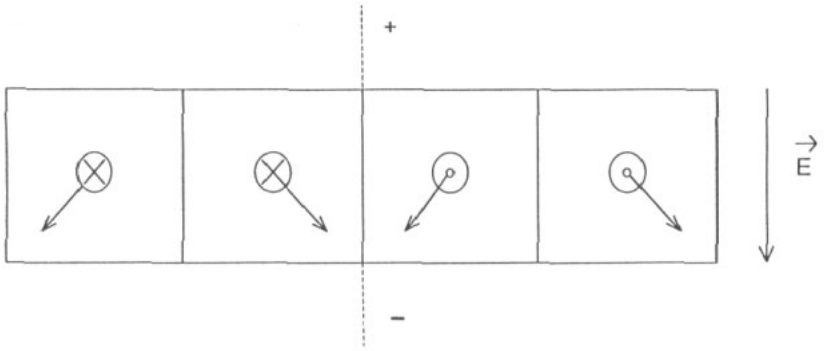

(b)

Figure 2. (a) Diffraction pattern recorded at 60 K when a 4 kV cm^{-1} electric field is applied to the crystal along the [010] direction. (b) Picture describing the persistence of domain walls in the rhombohedral phase of KTN under an electric field. The directions ⟨111⟩ of the polar axis are indicated by arrows.

the large variety of birefringent domains gives rise to elliptic polarizations of all kinds. This explains the exchange of intensity from $I_{\parallel}$ to $I_{\perp}$ to a large extent. The sample, hence, acts as a polarization scrambler and produces virtually depolarized light.

In the rhombohedral phase the intensities $I_{\parallel}$ and $I_{\perp}$ have approximately the same values and remain constant in the whole temperature range. This hints at virtually constant domain sizes in the R phase.

2.2. *Dielectric permittivity and loss measurements*

The succession of phase transitions, which is evidenced by light diffraction and transmission (section 2.1) is very clearly revealed by dielectric measurements, which were performed with an impedance bridge HP4192A. Figure 4 shows both real and imaginary parts of the dielectric permittivity measured at a frequency $f = 2$ kHz on cooling and heating in the 60 K $\leqslant T \leqslant$ 100 K temperature range. Peaks and shoulders in the curve $\epsilon'(T)$ mark the transition temperatures successively for C–T, T–O and O–R as $T_{c1} = 82.5$ K, $T_{c2}^{-} = 78.5$ K

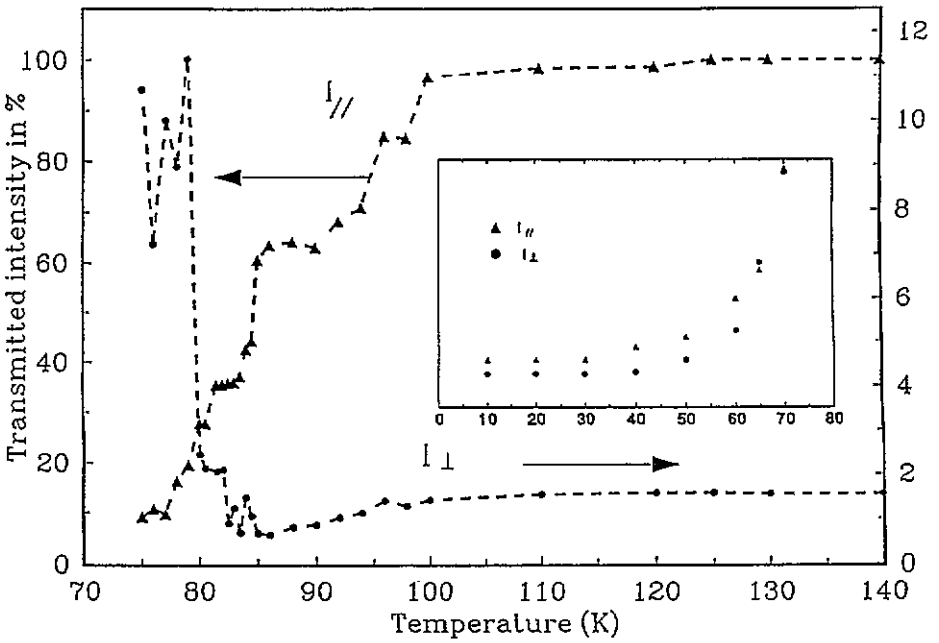

Figure 3. Temperature dependence of the transmitted light intensity through the KTN crystal between parallel ($I_{\parallel}$) or crossed polarizers ($I_{\perp}$). Note the difference in the scales. The inset concerns the values obtained in arbitrary units for the rhombohedral phase.

and $T_{c2}^{+} = 80$ K, $T_{c3}^{-} = 74.5$ K and $T_{c3}^{+} = 77$ K respectively (arrows in figure 4). The values obtained on cooling (T_{c1}, T_{c2}^{-}, T_{c3}^{-}) are close to those achieved from the light diffraction experiments (section 2.1). Slight hysteresis between heating and cooling runs confirms that the T–O and O–R transitions are first order.

The temperature behaviour of the permittivity in KTN with $x = 0.076$ is exactly analogous to that previously reported by Kind and Müller [20] in KTN with $x = 0.1$.

Connected with the ϵ' anomalies at T_{c1} and T_{c2}, the dielectric losses ϵ'' exhibit large increases, which appear as usual below the corresponding transition temperature. In the R phase, both ϵ' and ϵ'' display an additional shoulder at 72 K, which is probably connected with the domain transformation. The large increase of ϵ' in the cubic phase as the temperature decreases can be attributed to the formation of polar clusters, which rapidly increase in size. The peak of ϵ' at T_{c1} is clearly associated with the breaking of the cubic symmetry on a macroscopic scale. The decrease of ϵ' below T_{c1} reveals the increase of order in the ferroelectric phase. Dielectric losses, which are significantly larger in the T, O and R phases than in the C phase, indicate ferroelectric multidomain structures in the low-symmetry phases.

Curie–Weiss behaviour is evidenced in the plot it ϵ'^{-1} versus T in the cubic phase, as illustrated in figure 5. A linear best fit of the ϵ'^{-1} data within 125 K $\leqslant T \leqslant$ 175 K yields $T_c = 83.8$ K, which lies close to $T_{c1} = 82.5$ K as obtained from light diffraction and from direct inspection of $\epsilon'(T)$. Closer examination of ϵ^{-1} data within 100 K $\leqslant T \leqslant$ 125 K results in a non-classical critical behaviour $\epsilon' \propto (T\text{-}T_c)^{-\gamma}$ with $\gamma \sim 1.4$. A similar departure of the critical exponent from $\gamma = 1$ was reported in [20].

Figure 6 displays the frequency dependence of ϵ' and ϵ'' between 300 and 10^6 Hz for various temperatures. Upon cooling between 210 and 85 K, ϵ' is essentially independent of

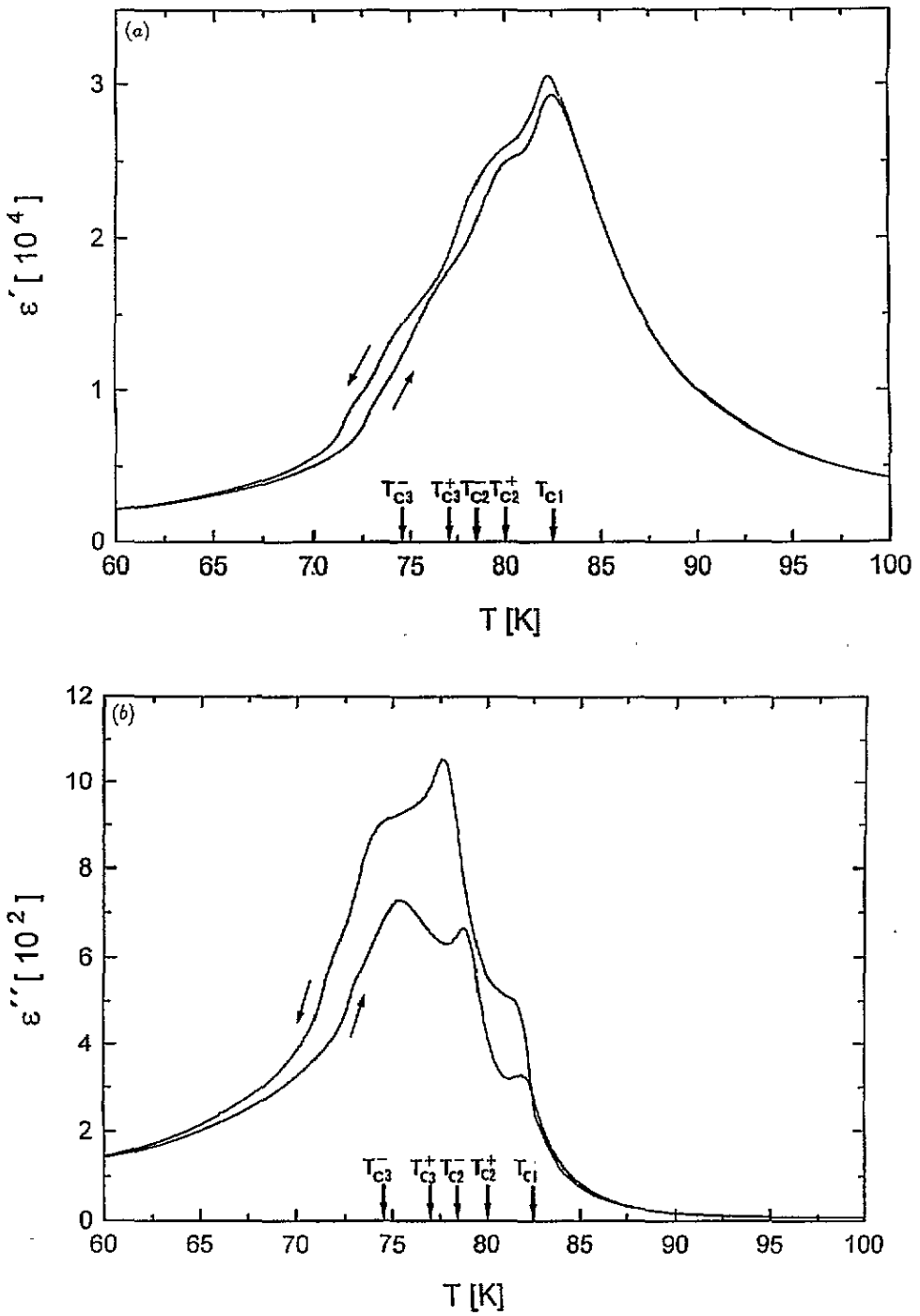

Figure 4. Real (a) and imaginary part (b) of the dielectric permittivity measured in KTN ($x = 0.076$) at $f = 2$ kHz on cooling and subsequent heating as indicated by arrows with a rate $|dT/dt| \sim 0.01$ K s^{-1} between 60 and 100 K. The transition temperatures T_{c1}, T_{c2} and T_{c3} on cooling (−) and heating (+) are marked by arrows.

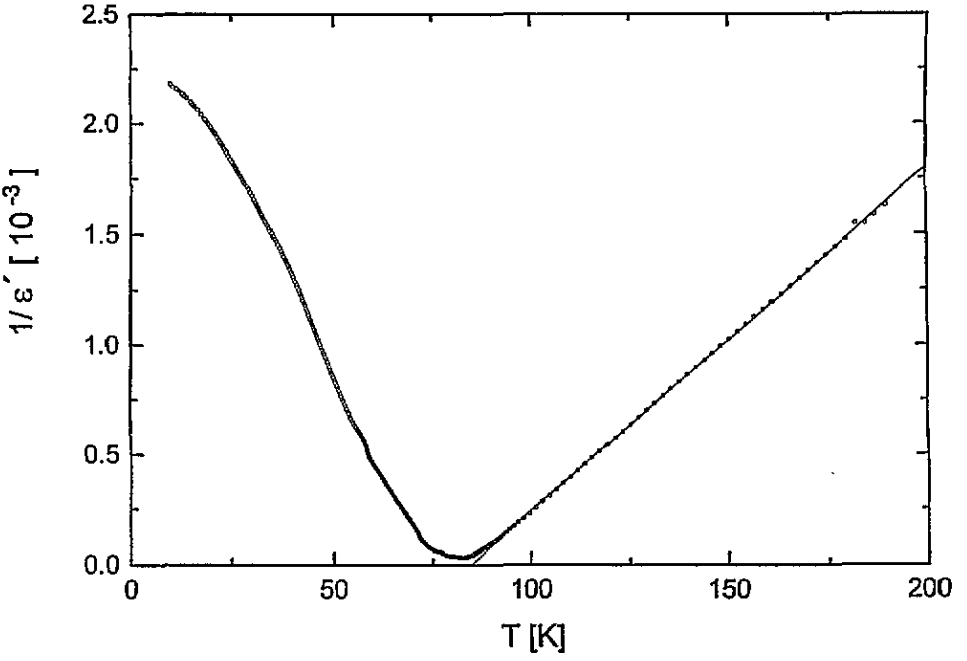

Figure 5. ϵ'^{-1} versus T measured in KTN at $f = 2$ kHz upon slow cooling (figure 4(a)) and fitted to a Curie–Weiss law with $T_{c1} = 83.82$ K (solid line).

frequency. A slight decrease of ϵ' with increasing frequency appears in the direct vicinity of T_{c1} ($T \sim 83$ K; curves 3 and 4) reflecting a dispersion step at higher frequency. Consistently, a dramatic increase of ϵ'' is observed in the same frequency region when approaching T_{c1}.

Presumably this feature is due to cluster response accompanying the precursor order phenomenon of the phase transition in the cubic phase. Just below T_{c1}, the flat behaviour of $\epsilon'(f)$ is replaced by a continuously decreasing function, approximately linear in $\log_{10} f$ (up to $f = 1$ MHz). In accordance with this dependence ϵ'' displays a broad peak in the T and O phases. This polydispersive low-frequency behaviour can be attributed to a wide distribution of domain walls [4,21] which gives rise to a broad distribution of relaxation times. Domain wall dynamics is predominant in the temperature range covered by the T and O phases. It still persists in the R phase (curves 8–11), but gradually weakens because of continuous domain growth upon cooling.

2.3. Raman measurements

2.3.1. Analysis of the spectra obtained in the whole frequency range. Light-scattering measurements are performed in right angle geometries using the 632.8 nm exciting line of an He–Ne laser. Spectra are recorded with a Spex double monochromator and a photon counting system. Depolarized Raman spectra are recorded as a function of temperature. The characteristics, i.e. the maximum and the width, of each Raman line are determined and its integrated intensity is carefully calculated. Therefore, in order to study the behaviour of the Raman line intensities as a function of the temperature, spectra are measured under the same experimental conditions. These conditions are only changed when we record the measurements at low frequencies instead of the data obtained in a complete frequency range.

Raman spectra recorded in the large frequency range are plotted for various temperatures in figure 7. At 140 and 100 K the spectrum displays large and intense bands, which are

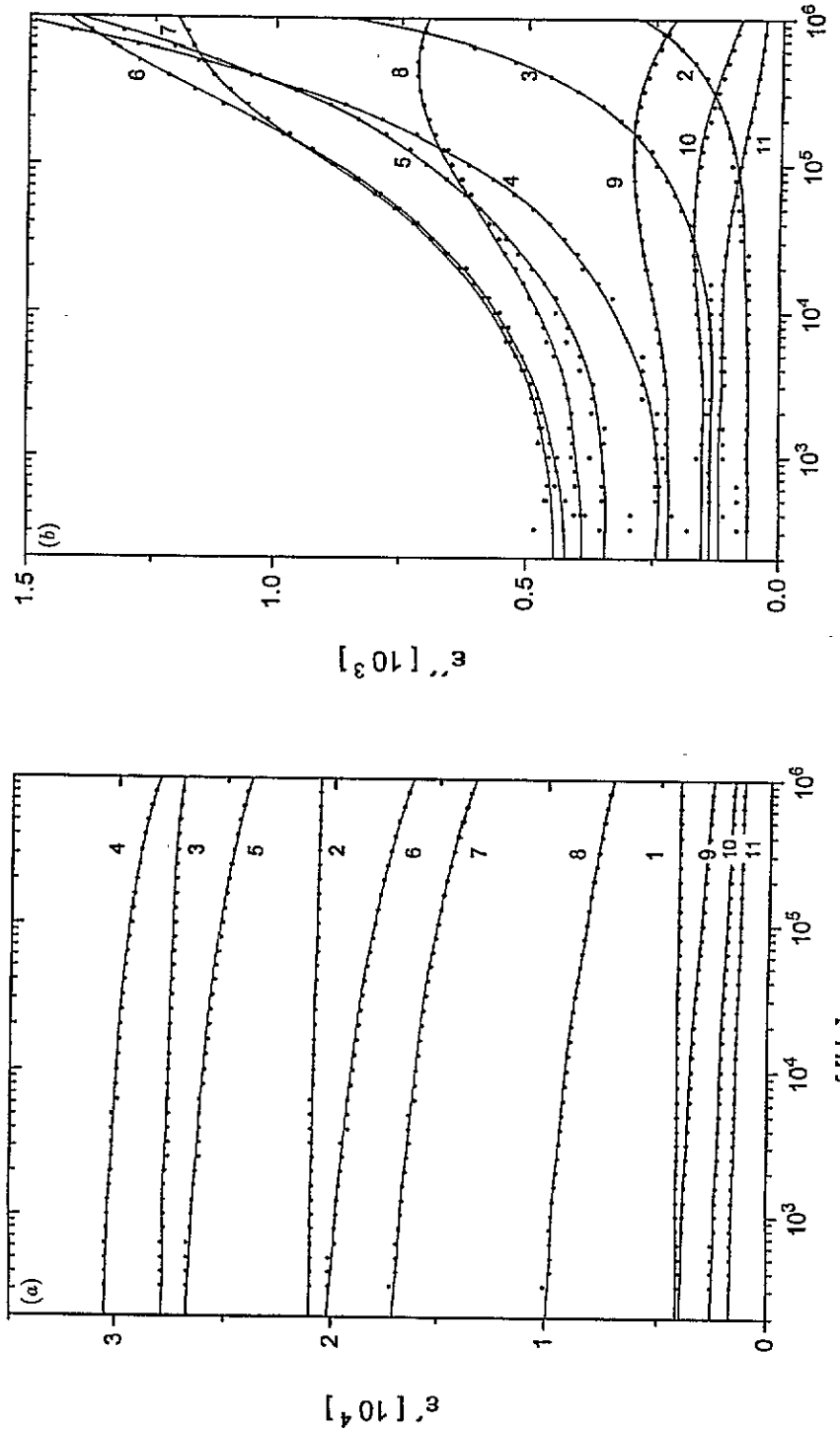

Figure 6. Real (a) and imaginary parts (b) of the dielectric permittivity measured in KTN ($x = 0.076$) at $T = 100$ (curve 1), 85.1 (curve 2), 83.2 (curve 3), 82.0 (curve 4), 79.9 (curve 5), 76.8 (curve 6), 75.0 (curve 7), 72.0 (curve 8), 66.2 (curve 9), 60.0 (curve 10) and 55.0 K (curve 11) at frequencies 300 Hz $\leqslant f \leqslant 10^6$ Hz. Data points are connected by eye-guiding lines. ε'' versus f at 100 K coincides with the abscissa axis and is not plotted explicitly.

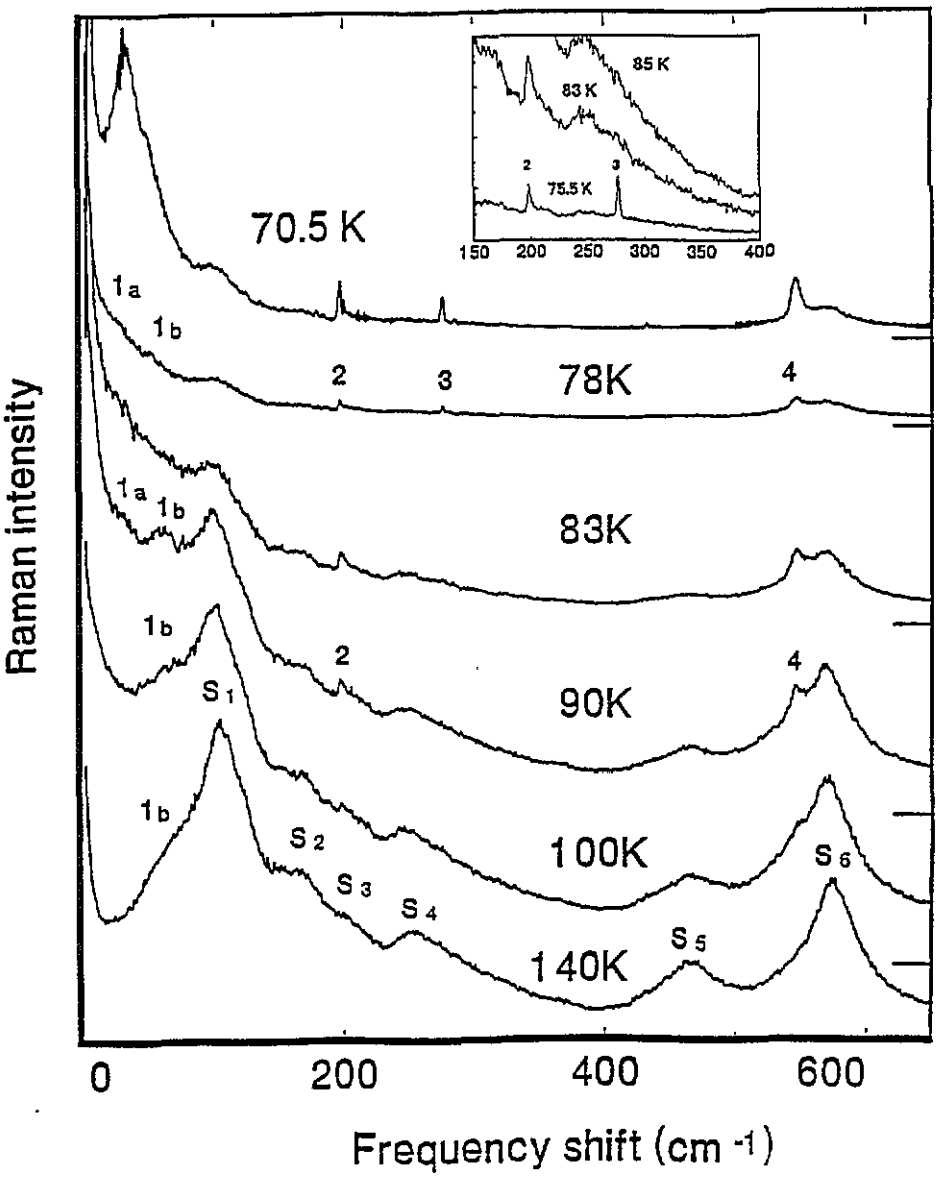

Figure 7. Whole Raman spectra in KTN with $x = 0.076$ recorded at various temperatures. The inset shows the occurrence of the line 3 (= TO3) at a temperature close to $T_{c1} \sim 83$ K. the horizontal lines indicate the base line for each spectrum.

known to be caused by second-order scattering processes [22] and therefore labelled S. The assignment of each line has been perfectly determined for pure $KTaO_3$ in the framework of a lattice dynamical model [23]. These bands appear in our KTN crystal at approximately the same frequencies as in $KTaO_3$ so the considerations used for $KTaO_3$ [22] still remain valid [24]. Among the second-order bands, only the peak position of S_1, which is attributed to the two transverse acoustic phonon scattering, displays a weak temperature dependence. All of these bands show a remarkable decrease in intensity when the temperature is lowered, especially below 85 K, so only the peaks S_1 and S_6 still exist in the spectrum recorded at

70.5 K.

Above $T = 82.5$ K, which corresponds to the C–T phase transition according to our light diffraction and dielectric data, the Raman spectrum exhibits some additional shoulders or peaks beside the intense second-order bands. These new lines cannot arise either from first-order phonons, which are in principle forbidden in the C phase, or from normal second-order processes, which were previously clearly determined. Some of these lines were earlier observed by Yacoby [25] for $x = 0.06$, by ourselves for $x = 0.02$ and $x = 0.09$ [9] and $x = 0.04$ [26] as well as by Toulouse *et al* for $x = 0.012$ [11]. These last authors focused their attention on the high-frequency lines, the so-called hard modes, and their evolution with temperature in the case of low Nb concentration. Here we study the possible relationship between the behaviour of these hard modes as well as that of the low-frequency lines and the quasi-elastic scattering at the successive phase transitions occurring in KTN crystals with high concentration.

In figure 7 the lines are labelled with increasing frequency. The lines 1-a and 1-b are clearly seen below 90 K. They lie in the 30–70 cm^{-1} frequency range and are probably hidden in the shoulder of the S_1 peak which is more intense and largely asymmetric for $T = 100$ and 140 K. The lines 2 and 4 occur below 90 K and are located around 200 and 545 cm^{-1} respectively.

As shown in the inset of figure 7, the line 3 arises at a temperature close to T_{c1}, in contrast to the other lines 1, 2 and 4, which exist well above T_{c1}. The decrease in intensity of each line, when the temperature passes through the C–T–O successive phase transition (between 85 and 76 K), is probably connected with the appearance and growth of the ferroelectric domains. In contrast, below T_{c3}, in the R phase the intensities display a surprising increase when the temperature is lowered. In this phase the lines are sharp and are clearly located at frequencies corresponding to the first-order phonons.

In order to analyse more clearly these experimental observations and to study their possible relation with the phase transitions, we calculate the integrated intensity J of each line as a function of temperature. The low-frequency lines denoted 1-a and 1-b merit a special treatment. Indeed, they are not well defined in the Raman spectrum recorded in the large frequency range and are also obscured by a quasi-elastic scattering that appears below 120 K and increases in the vicinity of T_{c1}. Therefore both the quasi-elastic scattering and the lowest-frequency lines are also measured in better resolution conditions and the results are described below in a separate part.

We calculate the integrated intensity of each peak from the equation

$$J = \int_a^b \frac{I(\omega)}{\omega[n(\omega)+1]}\,d\omega = \int_a^b I_R(\omega)\,d\omega \tag{1}$$

where $I(\omega)$ denotes the experimental scattering intensity, and $n(\omega)+1$ the Bose–Einstein population factor for the Stokes scattering. a and b correspond to the low- and high-frequency limits of the peak. In these calculations, the second-order scattering contribution and the background are eliminated. Some examples of corrected spectra and calculations are shown in figure 8. For instance (see figure 8(f)) the lines 4 and S_6 are decomposed by assuming two Lorentz profile functions and a weak constant background signal. Good agreement is achieved between experimental data and the calculated spectra.

The temperature dependence of the intensities J is reported in figure 9 for each hard mode. The comparison of these curves leads to the following remarks. The peaks 2 and 4 occur well above T_{c1}, whereas the line 3 appears only close to T_{c1}. The appearance of J (peak 3) coincides with the first maximum of J (peak 2) at 83 K (close to T_{c1}). J (peak 2)

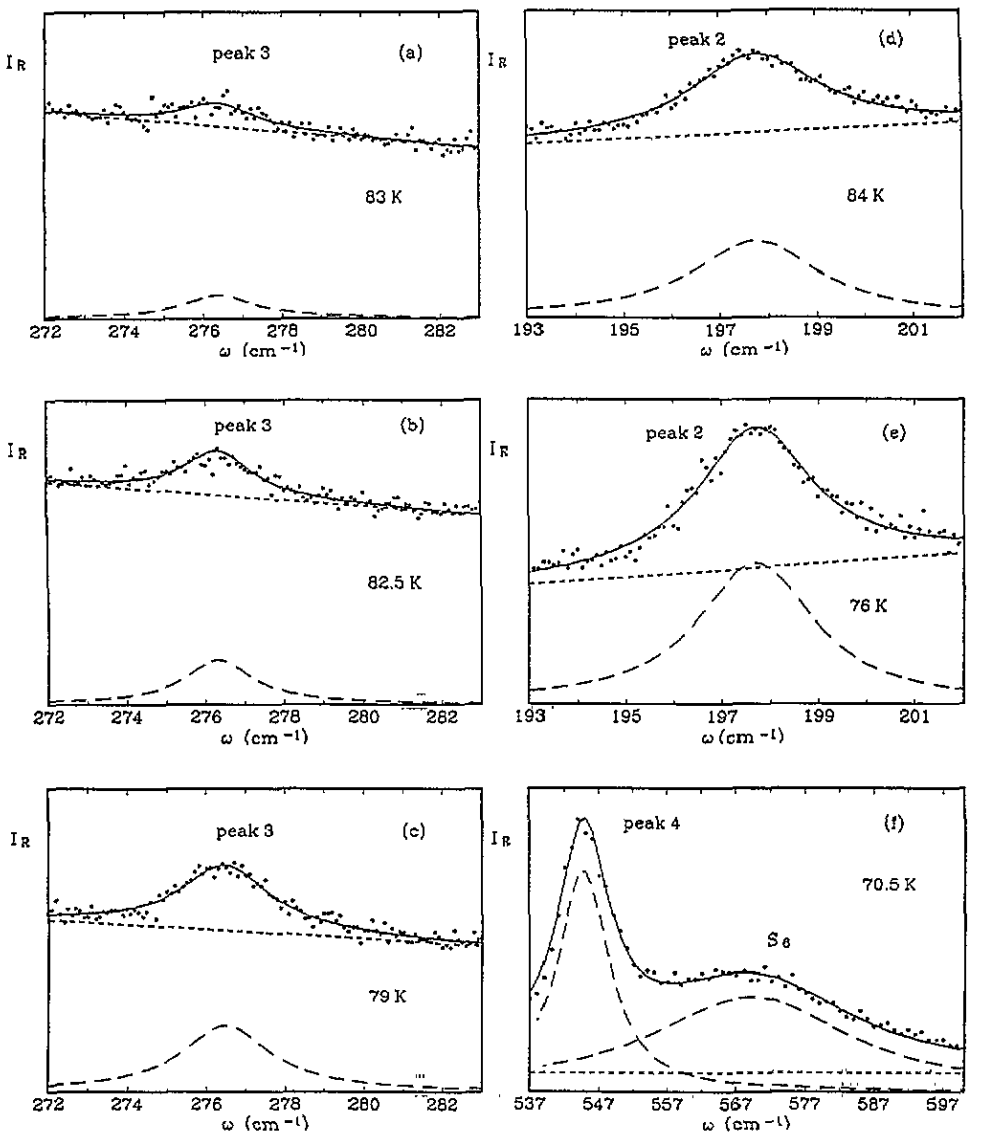

Figure 8. Raman intensity I_R as calculated according to equation (1) for the lines 2, 3 and 4. The dots correspond to the experimental data. The continuous lines are the spectra fitted with a damped harmonic oscillator model. The dashed curves are calculated spectra, corrected by the second-order scattering and the background (dashed line) as approximated by a second-order polynomial.

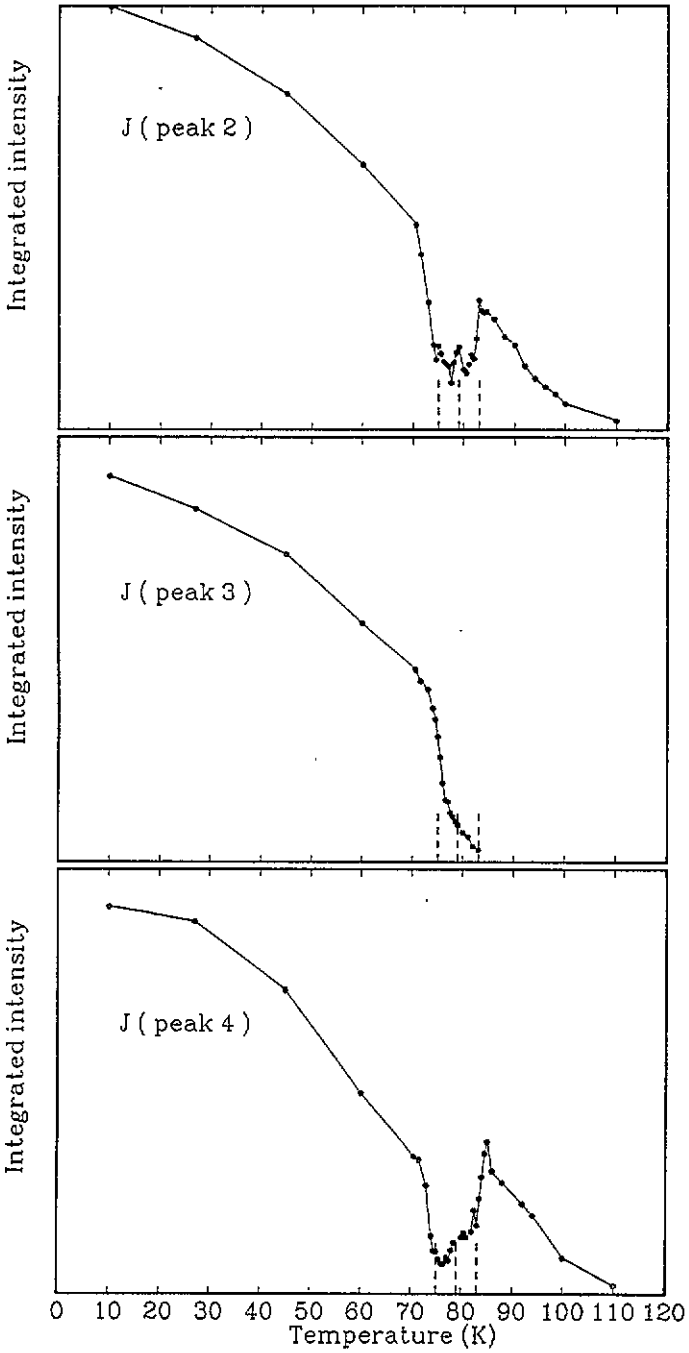

Figure 9. Integrated Raman intensities of the lines 2, 3 and 4 as functions of the temperature in $KTa_{0.924}Nb_{0.076}O_3$. The transition temperatures T_{c1}, T_{c2} and T_{c3} as determined from light diffraction and dielectric data, are marked by dashed lines. The solid lines are guides to the eyes.

displays three maxima at 83, 79 and 75 K, i.e. very close to the transition temperatures T_{c1}, T_{c2} and T_{c3}, respectively. J (peak 4) shows similar but less pronounced anomalies at the same temperatures, whereas the peak 3 displays a large jump-like increase at 75 K. In the T and O phases (74 K $< T <$ 85 K) the behaviour of J (peak 2) and J (peak 4) is very similar, but different from that of J (peak 3), whereas all intensities exhibit a very similar continuous increase in the R phase below T_{c3} with decreasing temperature.

2.3.2. Analysis of the low-frequency spectra. The low-frequency spectrum is reported in figure 10 for several temperatures in the different phases. Intense quasi-elastic (QE) scattering can be clearly observed when the temperature decreases on approaching T_{c1} (83 K). This scattered intensity may be discerned from Rayleigh elastic scattering by the change in the slope of the profile around 5 cm^{-1}. It should be noticed that the low-frequency region below 20 cm^{-1} remains constant between 300 and 140 K and that QE scattering clearly appears below 120 K. The QE intensity increases on cooling, reaches a maximum at 82.5 K $\sim T_{c1}$, then decreases and vanishes around 60 K. The scattered intensity between the QE line and the peak S_1 increases monotonically between 100 and 86 K. Below 86 K two broad bands denoted as 1-a and 1-b emerge from this scattered intensity and become more resolved when the temperature decreases. As the temperature is lowered below T_{c3} (about 75 K) these peaks increase significantly in intensity and shift up in frequency. They are assigned to the E and A_1 components of the lowest frequency (TO_1) phonon in the R phase.

To illustrate these observations the integrated intensities of the QE scattering and of the low-frequency peaks (1-a and 1-b) are plotted in figure 11 together with the behaviour of the intensity of the two-phonon peak S_1. In contrast to the case of the high-frequency peaks, the integrating limits a and b in equation (1) now depend on the lineshape and thus on the temperature. Figure 11 shows that J(QE) increases significantly on cooling, exhibits a principal maximum for a temperature close to T_{c1}, then decreases through the T–O and O–R phase transitions with slight step-like anomalies. Below 60 K, in the R phase, J(QE) has a nearly constant value. It is noticed that the real dielectric permittivity ϵ' at 2 kHz (given in figure 4) and J(QE), which gives the total dielectric response at higher frequency, exhibits a very similar behaviour as a function of the temperature. The intensity J (peak 1) successively presents a maximum and a minimum at 84 and 76 K, close to T_{c1} and T_{c3} respectively. On decreasing the temperature in the R phase J (peak 1) recovers and displays a constant value. The abrupt decrease of intensity between 84 and 76 K occurs within the range of the T and O phases. On cooling $J(S_1)$ exhibits a large decrease between 90 and 75 K then a slight diminishing in the R phase. The intensity for the other second-order bands, not reported here, shows a similar behaviour with temperature.

In order to extract the characteristics of the lowest-frequency TO1 mode, and of the QE scattering in the various phases, we adjust the low-frequency profile with a model based on the coexistence of a relaxational central peak and three oscillators corresponding to the peaks 1-a, 1-b and S_1. Figure 12 illustrates the analysis of the spectrum recorded at 70 K. Good agreement is achieved between the experimental data and the calculated values. Results obtained for the frequency and width of the soft phonon are reported in figure 13. Three distinct temperature ranges can be considered for both low-frequency lines. Below T_{c3} in the R phase, lines 1-a and 1-b corresponding to the E(TO1) and A_1(TO1) phonons respectively show the usual behaviour of the soft modes in a ferroelectric phase: the frequency diminishes and the damping increases when the temperature approaches the phase transition temperature (R–O). According to the description given earlier for $KNbO_3$ [27], the E(TO1) and A_1 (TO1) are both the stiffened components in the 'last' rhombohedral phase of the soft mode in the cubic phase, since their frequencies increase and saturate

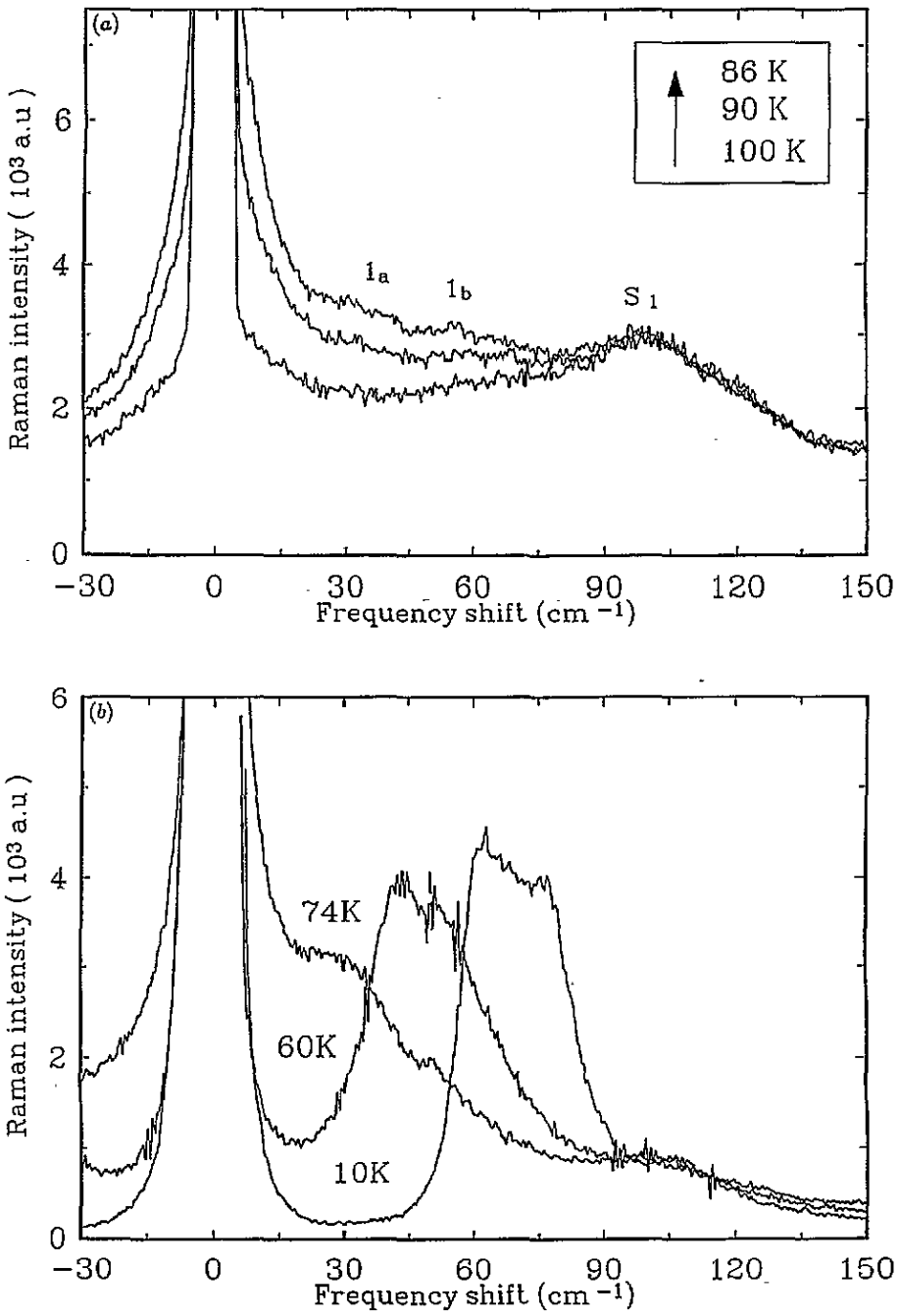

Figure 10. Low-frequency Raman spectrum recorded at various temperatures in KTN (x = 0.076).

on decreasing temperature. In the cubic phase, above 85 K, frequency and damping are relatively large and independent of temperature. This completely disagrees with the soft phonon picture. In fact, above T_{c1} the broad lines 1-a and 1-b should rather correspond to a phonon density of states and the characteristics deduced from the Lorentzian fitting in this

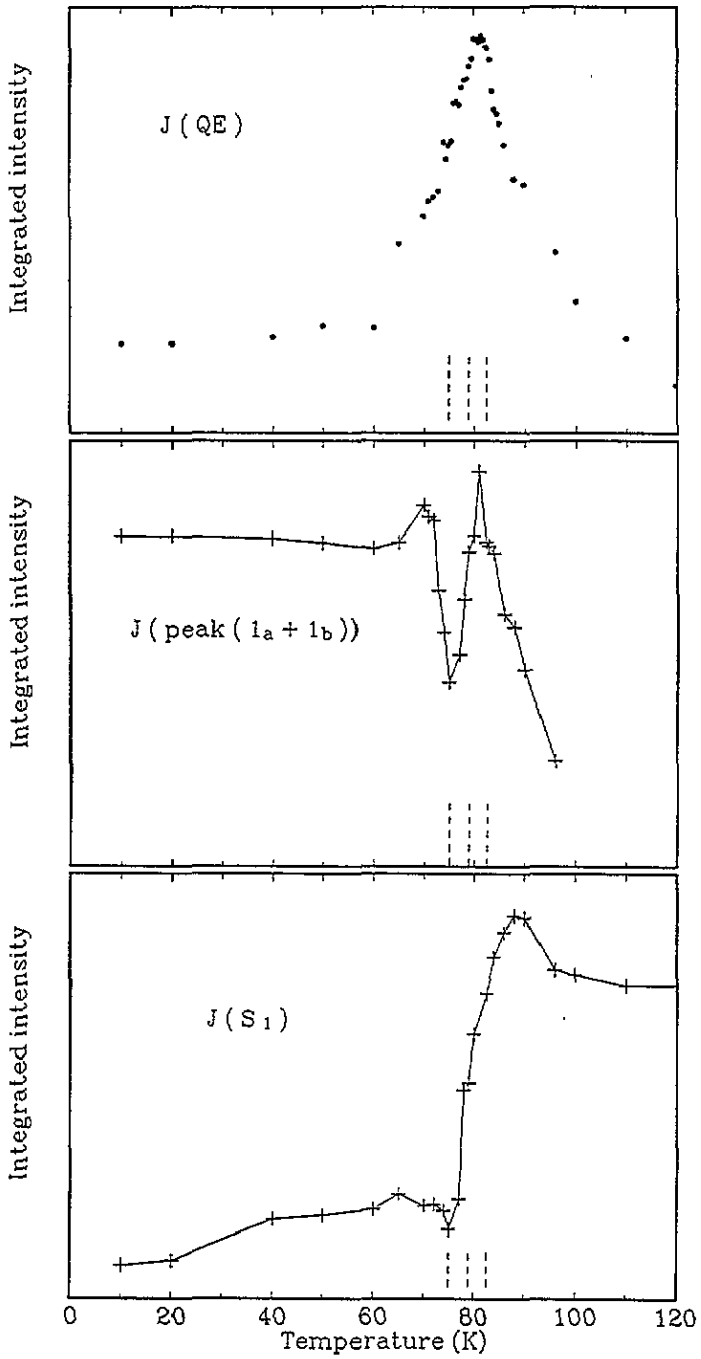

Figure 11. Temperature dependence of the integrated intensity for the quasi-electric scattering, J(QE), the low-frequency peaks, J(1-a+1-b), and the second-order line, $J(S_1)$.

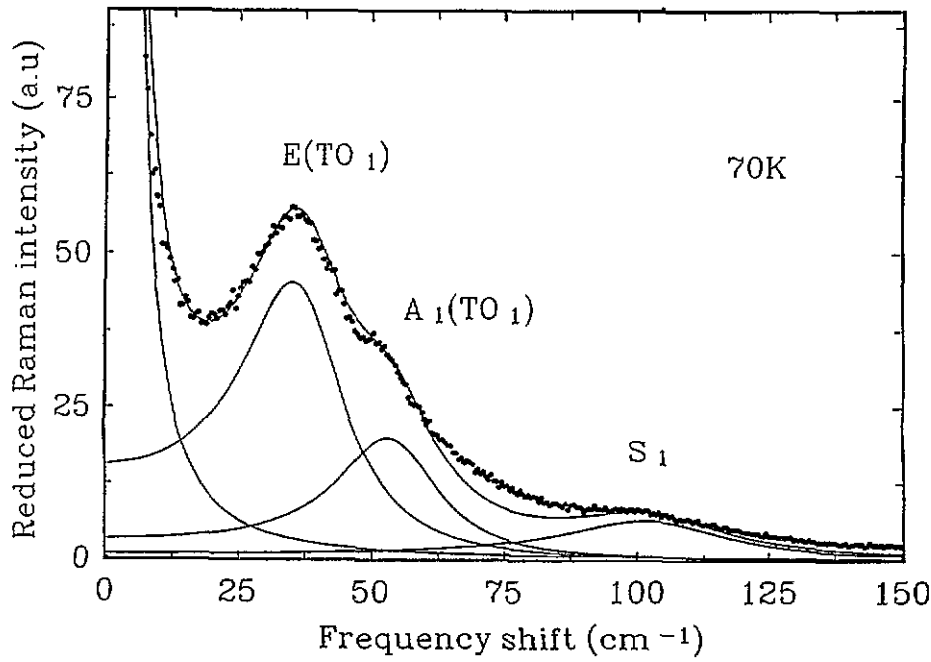

Figure 12. Low-frequency reduced Raman spectrum recorded at 70 K (R phase). The spectrum is fitted to a model based on the coexistence of a central relaxational peak and damped oscillators corresponding to the peaks 1-a, 1-b and S_1. Experimental data are represented by points.

phase cannot be identified with the frequency and damping of a specific phonon. Therefore the large decrease of the linewidth on cooling through the intermediate temperature range covered by the T and O phases is probably connected with the fact that the density of states is progressively replaced by first-order phonons in the non-cubic phases. Therefore the broad lines (1-a and 1-b) observed at low frequency well above T_{c1} cannot be attributed to usual first-order phonons.

3. Interpretation

Light diffraction and dielectric permittivity measurements in KTN with $x = 7.6\%$ clearly reveal several structural changes on a macroscopic scale, which in addition are accompanied by the appearance of ferroelectric domains. This KTN crystal thus does undergo the C–T–O–R transformations. These transitions are prepared by precursor effects in the C phase as evidenced by light transmission, dielectric and QE scattering experiments. The observation of forbidden lines in the Raman spectrum has to be interpreted in relation to these precursor phenomena.

The occurrence of intense QE scattering on approaching T_{c1} in the present study as well as for other [8, 9] concentrations, together with the dielectric dispersion above 1 MHz [10], indicate the presence of correlated relaxing dipoles within clusters. Since they are randomly distributed, the clusters formed around Nb ions give rise to zero average polarization of the C phase. As revealed by the rapid increase of J(QE) and ϵ' on approaching T_{c1}, these clusters grow as the temperature decreases and induce the transition in the T phase at T_{c1}. The existence of precursor clusters can also explain the decrease of the transmitted light intensity in the C phase. On the other hand, the light diffraction experiments clearly show

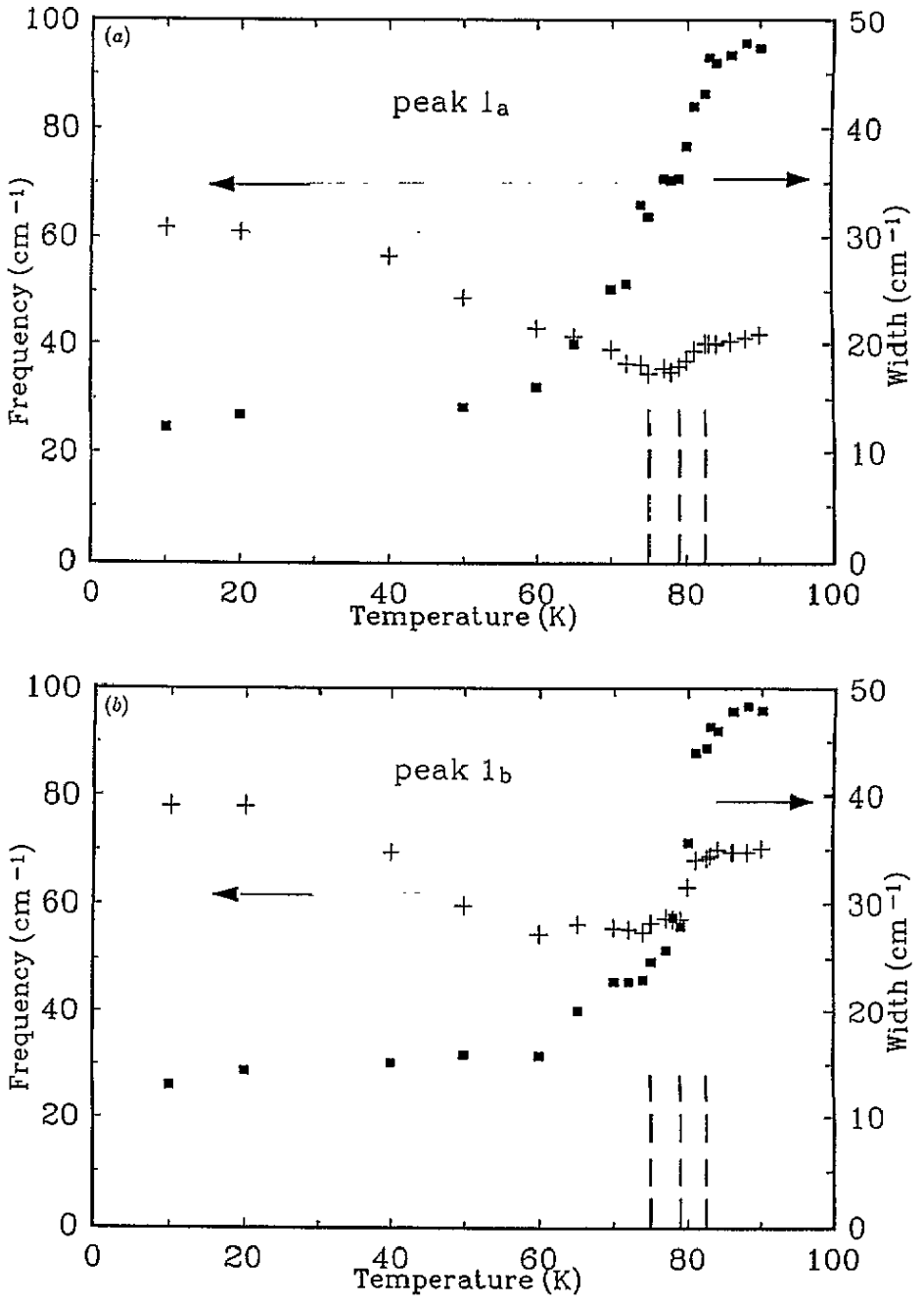

Figure 13. Temperature dependences of the frequencies and widths of the peaks 1-a and 1-b through the successive phase transitions.

that the crystal retains C symmetry on a macroscopic scale, since no quadrupolar domains are observed.

Now we turn to the interpretation of the Raman spectra. The lines 1, 2 and 4, which are detected well above T_{c1} are attributed to phonon density of states activated by relaxing

Nb ions in the C cell. An alternative interpretation might arise from the local breaking of the C symmetry, which should give rise to the detection of zone centre phonons. Indeed, the lines 2 and 4, appearing well above T_{c1} as well as the line 3 occurring at T_{c1} are located at frequencies close to those of the corresponding first-order phonons detected below T_{c1}. However, this hypothesis is discarded here for the following reasons: (i) our measurements do not provide any indication of domains or non-cubic symmetry above T_{c1}; (ii) the band 1, which occurs simultaneously with the lines 2 and 4, is very broad and located at a frequency larger than the corresponding transverse optical phonon for zero wavevector. Also the lines 2 and 4 are wider above T_{c1} than below T_{c1}. This broad lineshape is more consistent with the phonon density of states picture.

The apparent difference between the widths of the line 1 and those of the lines 2, 3 and 4 arises from the dispersion of the corresponding branches [24]. The phonon curves issued from the transverse optical phonons TO2, TO3 and TO4 are relatively flat whereas the soft phonon branch exhibits a large dependence onthe wavevector. In addition, this optical branch strongly interacts with the transverse acoustic branch [28]. The presence of additional lines above T_{c1} in the C phase is therefore attributed to the activation of phonons with wavevectors q belonging to the whole Brillouin zone. Lines 2 and 4 arise from flat branches whereas the broad lines 1-a and 1-b are issued from largely dispersive TA and TO1 branches. The simultaneous appearance and increase of J(EQ) and additional lines (1,2 and 4) above T_c clearly reflect that the phonon densities of states are activated by the dynamical disorder connected with relaxing dipoles. The special behaviour of line 3, which appears only close to T_{c1}, can be related to the non-polar character of the TO3 optical phonon, as suggested in [11]. In our investigations it is shown that the occurrence of line 3 coincides with the detection of diffraction spots and thus with the appearance of non-cubic structural domains.

Whereas the behaviour of the QE scattering intensity reflects the dynamics of the clusters, the dependence of the Raman line intensities gives information on the correlation length. As the temperature is lowered between T_{c1} and T_{c3} (i.e. 82.5 and 75 K), an increase of the correlation length is expected, resulting from a blocking of the cluster relaxation, clearly revealed by the diminishing of both the intensity J(QE) and the permittivity ϵ'. The decrease of J (peak 1) that is in fact observed is probably related to the decrease of the total transmitted intensity (figure 3) due to domains in the intermediate phases. The broad distribution of the relaxation times characteristic of the domain wall response is revealed by the wide dependence of the dielectric losses ϵ'' versus frequency in this temperature range.

Below the lowest phase transition temperature T_{c3}, in the R phase, the increase of all intensities J and the decrease of ϵ' and ϵ'' as a function of the temperature confirm the existence of a collective ordering of the Nb ions in this phase. The domains grow with decreasing temperature and finally stabilize in size. This explains the constant value of both the integrated scattering intensity J (peak 1) and of the transmitted intensity at the lowest temperatures. Finally, the disappearance of the domain relaxation, which corresponds to the flat behaviour of ϵ' versus $\log_{10} f$ and the constant value of J(QE) below 50 K is explained by the gradual growth of large domains.

4. Conclusion

Successive cubic–tetragonal–orthorhombic–rhombohedral structural changes in the $KTa_{0.924}Nb_{0.076}O_3$ crystal are clearly revealed by light diffraction measurements. The temperatures of the phase transitions are found to be very close to those corresponding to anomalies in the dielectric behaviour. Precursor effects above these transition temperatures are revealed

by the observation of Raman lines. They are clearly related to polar clusters identified by quasi-electric scattering. The presence above T_{c1} of Raman lines, which are located close to their positions below T_{c1}, is attributed to phonon densities of states activated by Nb centred clusters. This view is corroborated by a very recent theoretical study [29] which was made simultaneously with our present investigations.

The temperature dependence of the quasi-elastic scattering intensity is analogous to that of the permittivity. Our results support the description of the phase transition mechanism involving the coexistence of cooperative displacive ordering and reorientation of clusters, as for crystals with low concentration.

Acknowledgments

Thanks are due to A Klössner for technical help with the permittivity measurements. This work was supported by the Deutsche Forschungsgemeinschaft via Forschungsschwerpunkt 'Pseudosymmetrie' and the DAGIC division of the French Ministry of Education.

References

[1] Höchli U T, Knorr K and Loidl A 1990 *Adv. Phys.* **39** 405
[2] Vugmeister B E and Glinchuk M E 1990 *Rev. Mod. Phys.* **62** 993
[3] Rytz D, Höchli U T and Bilz H 1980 *Phys. Rev.* B **22** 359
[4] Sommer D, Friese D, Kleemann W and Rytz D 1991 *Ferroelectrics* **124** 231
[5] Höchli U T, Weibel H E and Boatner L A 1978 *Phys. Rev. Lett.* **41** 1440; 1977 *Phys. Rev. Lett.* **39** 1158
[6] Kugel G, Vogt H, Kress W and Rytz D 1984 *Phys. Rev.* B **30** 985
[7] Samara G A 1984 *Phys. Rev. Lett.* **53** 298; 1985 *Japan. J. Appl. Phys. Suppl.* **24-2** 80
Kleemann W, Schäfer F J and Rytz D 1985 *Phys. Rev. Lett.* **54** 2038
Gehring P M, Chou H, Shapiro S M, Hriljac J A, Chen D H, Toulouse J, Rytz D and Boatner L A 1992 *Phys. Rev.* B **46** 5116
[8] Lyons K B, Fleury P A and Rytz D 1986 *Phys. Rev. Lett.* **57** 2207
[9] Fontana M D, Bouziane E and Kugel G E 1990 *J. Phys.: Condens. Matter* **2** 8681
[10] Fontana M D, Maglione M and Höchli U T 1993 *J. Phys.: Condens. Matter* **5** 1895
[11] Toulouse J, Di Antonio P, Vugmeister B E, Wang X M and Knauss L A 1992 *Phys. Rev. Lett.* **68** 232
[12] Prater R L, Chase L L and Boatner L A 1981 *Phys. Rev.* B **23** 221
[13] Uwe H, Lyons K B, Carter H L and Fleury P A 1986 *Phys. Rev.* B **33** 6436
[14] Sokoloff J P, Chase L L and Boatner L A 1990 *Phys. Rev.* B **41** 2398
[15] Comes R, Lambert M and Guinier A 1968 *Solid State Commun.* **6** 715
[16] Toulouse J, Wang X M and Knauss L A 1991 *Phys. Rev.* B **43** 8297
[17] Fousek J and Janovec V 1969 *J. Appl. Phys.* **40**
[18] Courtens E 1981 *J. Phys. C: Solid State Phys.* **14** L37
[19] Kogelnik H 1969 *Bell Syst. Tech. J.* **48** 2009
Magnusson R and Gaylord T K 1977 *J. Opt. Soc. Am.* **67** 1168; 1978 *J. Opt. Soc. Am.* **68** 806
[20] Kind R and Müller K A 1976 *Commun. Phys.* **1** 223
[21] Kleemann W and Schremmer H 1989 *Phys. Rev.* B **40** 7428
[22] Kugel G E, Mesli H, Fontana M D and Rytz D 1988 *Phys. Rev.* B **37** 5619
[23] Migoni R, Bilz H and Bäuerle D 1979 *Phys. Rev. Lett.* **37** 115; Nilsen W G and Skinner J G 1967 *J. Chem. Phys.* **47** 1413
[24] Kugel G E, Fontana M D and Kress W 1987 *Phys. Rev.* B **35** 813
[25] Yacoby Y 1978 *Z. Phys.* B **31** 275
[26] Bouziane E, Fontana M D and Kugel G E 1992 *Ferroelectrics* **125** 331
[27] Fontana M D, Metrat G, Servoin J L and Gervais F 1984 *J. Phys. C: Solid State Phys.* **16** 484
[28] Fontana M D, Kugel G E, Foussadier L, Kress W and Rytz D 1993 *Europhys. Lett.* **23** 427
[29] Di Antonio P, Vugmeister B E and Toulouse J 1993 *Phys. Rev.* B **47** 5629